Buoyant mixing of miscible fluids of varying viscosities in vertical tubes

Marie Debacq, Jean-Pierre Hulin, Dominique Salin, Bernard Perrin, E. John Hinch

Buoyant mixing of miscible fluids of varying viscosities in vertical tubes

M. Debacq,[a] J-P. Hulin,[b] and D. Salin
Laboratoire Fluides Automatique et Systèmes Thermiques, UMR 7608, CNRS, Universités P. et M. Curie and Paris Sud, Bâtiment 502, Campus Universitaire, 91405 Orsay Cedex, France

B. Perrin
Laboratoire de Physique de la Matière Condensée, UMR 8551, CNRS, Ecole Normale Supérieure, Département de Physique, 24 rue Lhomond, 75231 Paris Cedex 05, France

E. J. Hinch
DAMTP-CMS, University of Cambridge, Wilberforce Road, CB3 OWA Cambridge, United Kingdom

(Received 6 June 2003; accepted 19 September 2003; published 5 November 2003)

Gravity-induced mixing of two fluids in long vertical tubes is studied experimentally as a function of the density contrast characterized by the Atwood number At (10^{-5} to 0.2), the fluid viscosity ν (1 to 16×10^{-6} $m^2\,s^{-1}$) and the tube diameter d (2 to 44 mm). At low density contrasts, a stable counterflow is observed over a large fraction of the tube and its region of existence increases at high viscosities and small tube diameters. For larger density contrasts, the flow is either convective or turbulent and the mean concentration profile $\overline{C}(x,t)$ follows a diffusive spreading law characterized by a diffusivity D. An unexpected increase of D and of the characteristic velocity V_f of random fluid motions is observed when ν increases. This results from the coarser mixing in more viscous fluids which increases local density contrasts and buoyancy forces. Dimensionless plots of the diffusion coefficient D/ν as a function of the Reynolds number of the flow indicate a transition between two different diffusive regimes. Scaling arguments are put forward to account for the dependence of V_f and of the characteristic diffusion length in the convective–diffusive regime. © *2003 American Institute of Physics.* [DOI: 10.1063/1.1624838]

I. INTRODUCTION

Gravity-induced mixing of miscible fluids of different densities stratified in an unstable configuration is associated with the development of Rayleigh–Taylor instabilities.[1–8] There are many examples of such instabilities in a variety of domains: astrophysics and nuclear fusion,[4,9] extraction columns in chemical engineering,[10] fire propagation in vertical shafts,[11] drilling and completion fluids in petroleum engineering. The dependence on time of the displacement of the front of the instability has been frequently studied at early times. After an initial exponential increase, the displacement is often quadratic with time at short times[6,7,12,13] and then linear.[12,14] In some numerical simulations a $t^{1/2}$ regime occurred before a transition to t^2. Self-similar flows with characteristic lengths increasing as $t^{2/5}$ have also been predicted.[15]

In the present paper we deal specifically with buoyant mixing in constricted geometries (i.e., tubes) for amplitudes of the Rayleigh–Taylor instability very large compared to the tube diameter. In similar configurations, mixing zone widths increasing approximately as $t^{1/2}$ have been reported by other authors.[10,11] Baird *et al.*[10] studied the mixing of a small volume of heavy salt solution dropped at the top of a tube filled with water. However, the time dependence of the concentration profile was not measured. Zukoski *et al.*[11] measured concentration profiles in such a configuration: this study was realized at long times where spreading is strongly influenced by the boundary conditions and the behavior at intermediate times was not investigated. In both experiments, the initial interface is located at one of the ends of the tube which makes the corresponding boundary condition more complex.

In a previous work,[16] we reported buoyancy-induced mixing in a long vertical tube (of single diameter 20 mm) for two miscible fluids with different densities in an unstable configuration but the same viscosity (10^{-6} $m^2\,s^{-1}$). The interface between the two fluids is initially at the middle height of the tube and the Atwood number At characterizing the density contrast ranged from 2×10^{-5} to 10^{-1} [$\mathrm{At}=(\rho_2-\rho_1)/(\rho_2+\rho_1)$ in which ρ_1 and ρ_2 are, respectively, the densities of the light and heavy fluids]. For $\mathrm{At}>10^{-4}$, the normalized concentration profiles (averaged over the tube section) are self-similar and can be superimposed by normalizing distance by the square root of time. In addition, these profiles can be fitted precisely by solutions of a diffusion equation: this allows us to characterize the phenomenon by a macroscopic diffusion coefficient D and confirms the spreading of the front as $t^{1/2}$.

This diffusivity D is many orders of magnitude (typically 10^5 times) larger than the molecular diffusion coefficient since this macroscopic mixing is induced by random fluid motions and not by molecular diffusion. A surprising feature is the very small increase of D (typically from 2×10^{-4} to 6×10^{-4} $m^2\,s^{-1}$) as At increases by 3 orders of

[a]Present address: CNAM, Chaire de Chimie Industrielle—Génie des Procédés 2 rue Conté, 75003 Paris, France.
[b]Electronic mail: hulin@fast.u-psud.fr

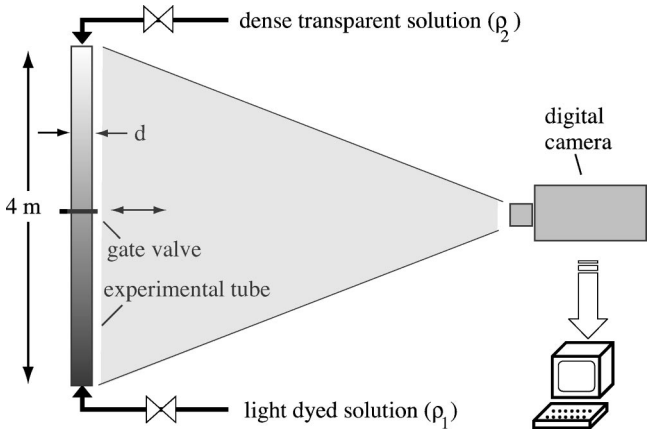

FIG. 1. Schematic view of experimental setup.

magnitude from 10^{-4} to 10^{-1}. The diffusivity D remains roughly constant up to $\mathrm{At}=5\times10^{-3}$ with a typical value 200 times that of the viscous diffusivity ν; it increases then roughly linearly with At for larger density contrasts. This differs from the complete change in the type of flow observed: it is turbulent for $\mathrm{At}\simeq10^{-1}$ while the instability patterns are much more organized for $\mathrm{At}\simeq10^{-4}$.

The first part of the present paper is devoted to a discussion of the main features of buoyancy-induced mixing regimes in 20 mm diameter tubes for fluids with a viscosity equal to that of water: the transition towards a nondiffusive flow regime at very low density contrasts will be of particular interest. This study will be extended to the domains of existence of the various flow regimes as a function of the fluid viscosity ν and of the tube diameter d. A quantitative analysis will then be achieved by studying the variations of D with At for different values of d and ν. Determining the velocities of the internal density fluctuations in the mixing zone and their dependence on At, ν and d will allow us to interpret these results.

II. EXPERIMENTAL SETUP AND PROCEDURE

Experiments are performed in 4 m high vertical transparent tubes of internal diameters $d=2$, 3, 5, 10, 20, and 44 mm with a sliding slot valve in the middle (Fig. 1). This large length allows us to perform easily measurements before the mixing zone has reached the end of the tube and thus to neglect their influence. The setup is illuminated from behind. The lighter fluid is water or a water–glycerol solution dyed with nigrosine (40 mg/L). The heavy fluid is a solution of either water or water and glycerol and of $CaCl_2$ salt at a concentration between 0.05 and 300 g/L. The viscosity ν of the two fluids is the same and chosen between 1 and 16 $\times10^{-6}$ $\mathrm{m^2\,s^{-1}}$ by varying the relative glycerol mass concentration in the solutions between 0 and 60%.

At the beginning of each experiment, the upper and lower halves of the tube are, respectively, filled with the heavy and light solutions. Mixing is initiated by opening the slot valve (which takes a few tenths of a second) and the typical duration of the measurements is 1200–1800 s. Video recordings of a small fraction (typically 30 cm) of the height of the tube close to the gate valve are also made to obtain a qualitative view of the flow.

Quantitative results are obtained by recording with a digital camera (1300×20 pixels) images of the tube centered on the gate valve. The images correspond to a tube length ranging from 1.8 m (for $d=2$, 3 and 5 mm) to 2.6 m (for $d=8$, 20 and 44 mm). An independent calibration is first realized by recording images with the tube filled with different solutions of constant, well defined concentrations: this calibration allows one to confirm that the light intensity varies exponentially with the dye concentration.

During the experiment, digital images are recorded at 1 or 2 s intervals and translated into concentration maps using the known calibration. They are then normalized by the values of the heavy (transparent) and the light (dyed) solutions. Finally, the normalized concentrations are averaged over the tube section at each height x to obtain the mean concentration profile $\overline{C}(x,t)$. These profiles are either used directly [Figs. 2(g)–2(i)] or grouped into spatiotemporal diagrams [Figs. 2(d)–2(f)] in which the gray levels reflect the normalized concentration (the vertical and horizontal coordinates correspond to the distance x and the time t). Compared to the concentration profiles, these diagrams provide additional information about the propagation of concentration fluctuations.

A few test experiments were performed with zero or weakly stabilizing density contrasts: no significant mixing occurred for several hours. Otherwise, the Rayleigh numbers,

$$R_a=\frac{\mathrm{At}\,g d^3}{\nu D_m}, \tag{1}$$

are always far above the threshold ($\mathrm{Ra}_c=67.8$) for RT instabilities.[2,17]

III. QUALITATIVE EXPERIMENTAL RESULTS

A. Dependence of flow regime on density contrast

Let us first discuss the qualitative experimental results obtained in the tube of diameter $d=20$ mm with $CaCl_2$–water and nigrosine–water solutions of viscosity equal to that of water.

Figures 2(a)–2(c) display sequences of images from direct video recordings at three different Atwood numbers typical of the flow regimes observed in the experiments.

Figure 2(a) ($\mathrm{At}=5\times10^{-2}$) corresponds to a weakly turbulent flow regime. It is characterized by fast, random motions of fluid particles of characteristic scale about 1 cm at velocities of a few mm/s over distances of the order of the tube diameter. There is no sharp boundary between the unperturbed fluids and the mixing zone. The concentration variations are relatively small across the flow section which indicates a rather effective mixing similar to eddy diffusion.[18]

At a lower Atwood number [$\mathrm{At}=8\times10^{-4}$ in Fig. 2(b)], the mixing is much less effective and the internal structure of the flow is more visible. The outer boundary of the mixing zone is clearly defined and marked by the front tip of the

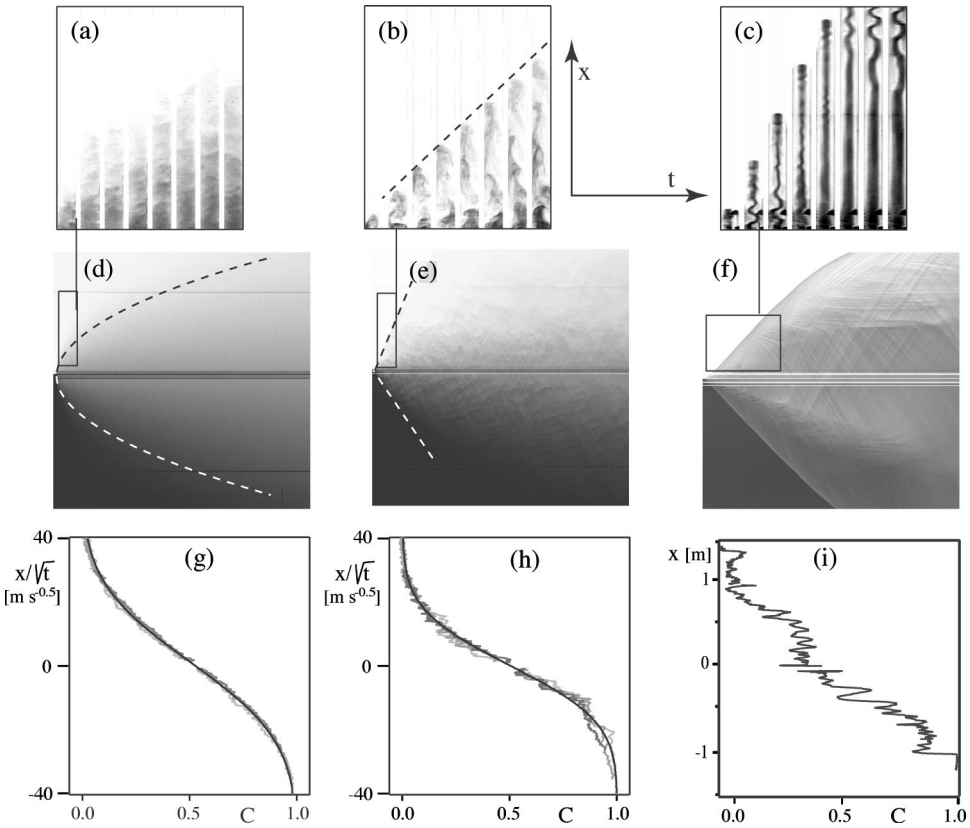

FIG. 2. (a), (b), (c) Sequences of images of a 30 cm high section of the tube right above the gate valve (at the bottom of the images) at respective decreasing Atwood numbers $\mathrm{At}=5\times10^{-2}$ (the time interval between images $\delta t=7$ s), $\mathrm{At}=8\times10^{-4}$ ($\delta t=5$ s), $\mathrm{At}=5\times10^{-5}$ ($\delta t=20$ s). (d), (e), (f) Spatiotemporal diagrams associated, respectively, to experiments (a), (b), and (c) (the vertical scale corresponding to distance along the tube and the horizontal scale to time). The vertical field of view is in all cases equal to 2.65 m and the time lapse covered to 1200 s. (g), (h) Normalized concentration profiles associated to experiments (a) and (b) ($t=120$, 360 and 960 s) and plotted as a function of $x/\sqrt{t}$. The continuous lines are best fits of the curves with an error function. (i) Normalized concentration profile plotted as a function of the height x ($t=190$ s).

fingering instability. The tip moves at a roughly constant velocity (dashed line) and its mushroom-like shape is typical of structures at finite Reynolds numbers where inertial forces are not negligible. Helical waves develop in the wake of the finger[19,20] due to the shear at the interface between the ascending and descending fluids. Fluid patches of higher density contrast [a darker color in Fig. 2(b)] propagate in the wake and move faster than the front tip. Their successive arrival at the front enhances the local concentration contrast there which tends to decrease through mixing with the surrounding fluid near the tip.

At a still lower Atwood number [$\mathrm{At}=5\times10^{-5}$ in Fig. 2(c)], mixing created by instabilities between the finger and the surrounding fluid is reduced: the tip is sharply visible and moves as before at a roughly constant velocity. The mushroom-like shape of the tip is less clear and the helical instability of the wake decays over after a few tube diameters (particularly at longer times). There results a stable counterflow region around the gate valve.

It will be seen below that these different structures of the flow result in very different mixing properties: in the two first regimes, efficient transverse mixing is induced by turbulence or by the wavy motions. In the third one, the two fluids flow side by side in opposite directions without mixing sideways.

Similar differences are observed on the spatiotemporal diagrams of Figs. 2(d)–2(f). In the turbulent regime [Fig. 2(d)], the boundary of the mixing domain is fuzzy and the gray level distribution is finely grained. The amplitude of the concentration fluctuations is also small, confirming the efficient mixing in that regime. The dotted lines correspond to relative concentrations of the heavy fluid, respectively, equal to 95% (the upper half of the diagram) and 5% (the lower half). Their parabolic shape is a first indication of an increase of the width of the mixing zone as $t^{1/2}$. At the lowest density contrast [Fig. 2(f)], the domain of stable counterflow corresponds to the region right above and below the gate valve; the well defined oblique streaks correspond to concentration fluctuations moving at a constant velocity all across this region. The height of this stable counterflow region is also observed to increase with time. Finally, the outer boundary of the mixing zone is very clearly visible. At the intermediate density contrast ($\mathrm{At}=8\times10^{-4}$), this outer boundary associated with the front tip is still visible [the dotted line in Fig. 2(e)]. Dark and light streaks marking internal motions of the fluid are more clear than in the turbulent case, confirming that mixing is coarser.

Figures 2(g)–2(h) demonstrate that the spreading of the mean concentration profile $\overline{C}(x,t)$ is diffusive at these two At values in spite of the strong qualitative difference between the two flow regimes. In both cases, the mean concentration profiles overlay very well when they are plotted as a function of $x/t^{1/2}$ and are, in addition, well fitted by an error function. This implies that $\overline{C}(x,t)$ satisfies the diffusion equation:

$$\frac{\partial \overline{C}(x,t)}{\partial t}=D\frac{\partial^2 \overline{C}(x,t)}{\partial x^2}. \tag{2}$$

Thus, D can be obtained in both regimes by fitting the experimental mean concentration curves to solutions of Eq. (2). In the following, we refer therefore to the regime of higher

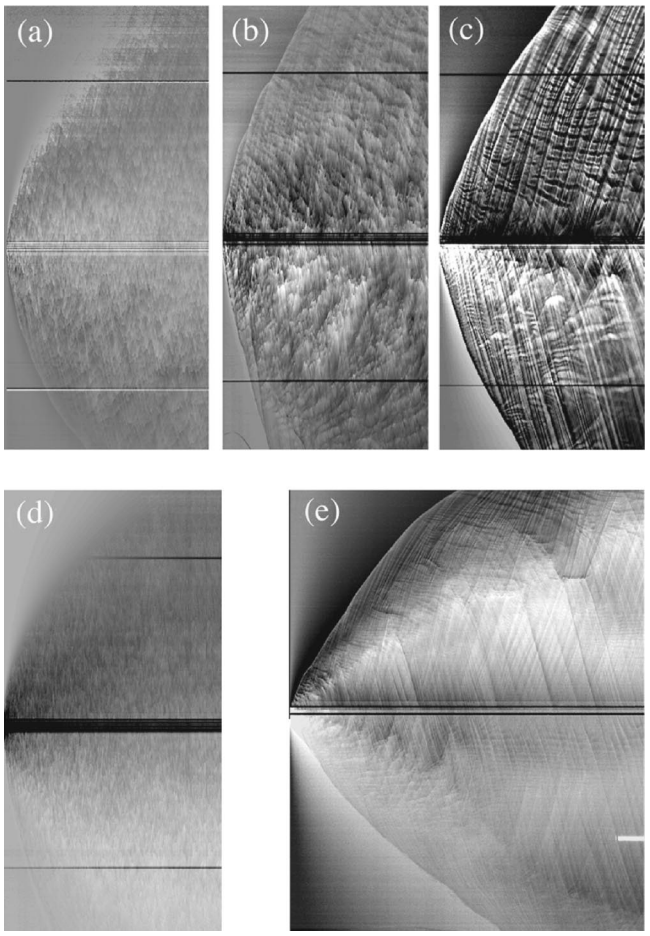

FIG. 3. (a), (b), (c) Spatiotemporal diagrams obtained for $d=20$ mm at a same density contrast $\mathrm{At}\simeq 3\times10^{-3}$ for three different viscosities: (a) $\nu=10^{-6}$ m^2 s^{-1}; (b) $\nu=2.3\times10^{-6}$ m^2 s^{-1}; (c) $\nu=16.3\times10^{-6}$ m^2 s^{-1}. (d), (e) Spatiotemporal diagrams obtained at a same density contrast $\mathrm{At}\simeq10^{-2}$ and viscosity $\nu=10^{-6}$ m^2 s^{-1} for two different tube diameters $d=20$ mm and $d=5$ mm. The vertical extension of the field of view is equal to 2.65 m for (a)–(d) and 1.8 m for (e). The time lapse covered is 1200 s for (a), (b), and (d), and 600 s for (c) and (e). In this figure, the global error function trend is substracted out from raw spatiotemporal diagrams and the gray level scale is amplified to enhance concentration fluctuations.

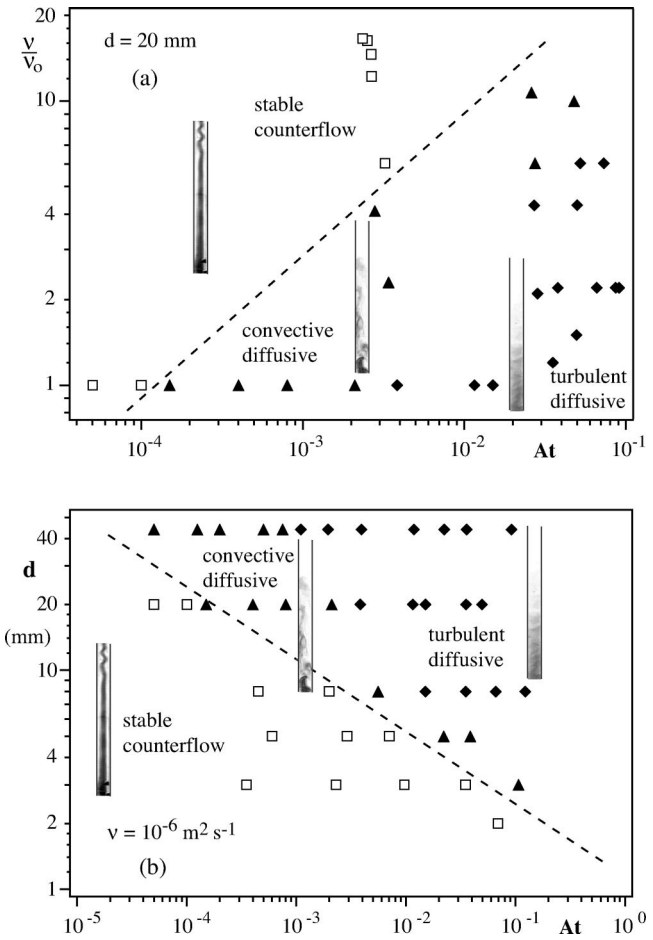

FIG. 4. Domains of observation of the various flow regimes (a) as a function of the fluid viscosity ν and of the Atwood number At ($d=20$ mm); (b) as a function of the tube diameter d and of the Atwood number At ($\nu=10^{-6}$ m^2 s^{-1}). (♦) Turbulent–diffusive regime; (▲) convective–diffusive regime; (□) stable counterflow regime. The dotted lines dividing the stable convective regime from the convective–diffusive regime correspond to power laws of exponents 1/2 in (a) and $-1/3$ in (b) and are discussed in Sec. V A 1. The more complex division between convective–diffusive and turbulent–diffusive is discussed in Sec. V D.

density contrasts as turbulent–diffusive and to the intermediate case as convective–diffusive. However, the concentration profile obtained at the lowest density contrast [Fig. 2(i)] clearly cannot be fitted by an error function due to the broad domain of constant average concentration below and above the gate valve. Note that this roughly constant concentration of order 0.5 does not reflect a complete mixing of the two fluids; on the contrary, they are completely separated, each occupying roughly half of the tube section.

B. Dependence of flow regime on viscosity

The above experiments all correspond to a viscosity $\nu=10^{-6}$ m^2 s^{-1}. Figures 3(a)–3(c) display spatiotemporal diagrams obtained for three different fluid viscosities $\nu=10^{-6}$, 2.3×10^{-6}, and 16.3×10^{-6} m^2 s^{-1} and for similar density contrasts ($\mathrm{At}\simeq3\times10^{-3}$). In the experimental range of Atwood numbers, the density of the mixture varies at most by 10%. For the sake of simplicity, the viscosity ν is therefore taken equal to μ/ρ_0 in which ρ_0 is the density of water and μ the dynamic viscosity of the solution. While the diagram obtained for $\nu=10^{-6}$ m^2 s^{-1} corresponds to a weakly turbulent mixing, that obtained for $\nu=2.3\times10^{-6}$ m^2 s^{-1} is typical of the convective–diffusive regime. For $\nu=16.3\times10^{-6}$ m^2 s^{-1}, streaks marking the internal motions of the fluid extend over very long distances, as for stable counterflows. These experiments have been repeated over a broad range of Atwood numbers At and viscosity values ν in order to confirm these trends. Figure 4(a) displays a map of the flow regimes identified as a function of At and ν. In all cases, increasing viscosity shifts the type of flow regime observed from turbulent–diffusive towards convective–diffusive and from convective–diffusive towards stable counterflow. This is in agreement with qualitative expectations that viscosity should damp out velocity fluctuations and reduce the local Reynolds number of the flow. The boundary between the stable counterflow and the diffusive regimes corresponds to At values proportional to ν^2. The transition between the

convective– and turbulent–diffusive regimes is quite smooth so that the values of At corresponding to the transition cannot be defined precisely.

C. Dependence of flow regime on tube diameter

The influence of the tube diameter d has been studied for $d=44$, 20, 8, 5, 3 and 2 mm. The influence of d is often quite drastic as can be seen in Figs. 3(d)–3(e) in which two spatiotemporal diagrams corresponding to a same (large) density contrast ($\mathrm{At}=10^{-2}$) and a same viscosity $\nu=10^{-6}$ m^2 s^{-1} are compared: while the flow regime is turbulent for $d=20$ mm, a well defined counterflow region is observed around the gate valve for $d=5$ mm. The same trend is observed in the map of Fig. 4(b) displaying mixing regimes observed as a function of At and d. Reducing d shifts the flow regime observed from turbulent–diffusive towards convective–diffusive and from convective–diffusive towards stable counterflow. The Atwood numbers corresponding to the transition between the convective–diffusive and stable counterflow regimes vary this time as d^{-3}. As above, the boundary between the convective– and turbulent–diffusive regimes cannot be defined precisely.

IV. QUANTITATIVE RESULTS

A. Macroscopic diffusion coefficients

1. Dependence on At and tube diameter

The macroscopic diffusion coefficient D is the key parameter characterizing the dynamics of mixing between the two fluids. It is determined by fitting with an error function the normalized mean concentration variation curves as shown in Figs. 2(g)–2(h). This procedure can of course only be applied in the turbulent–diffusive and convective–diffusive regimes. In a first step, the variation of D as a function of the Atwood number At has been studied for the three different tube diameters for which a clear diffusive regime was observed ($d=8$, 20 and 44 mm); the fluids always have the same viscosity $\nu=10^{-6}$ m^2 s^{-1} [Fig. 5(a)]. Experimental D values range between 10^{-4} and 2×10^{-3} m^2 s^{-1} and are much larger than the molecular diffusion coefficient (typically 10^{-9} m^2 s^{-1}). The coefficient D reflects indeed the random displacements of small fluid volumes with a size of a few mm or cm and not the thermal motion of individual molecules.

An important result is the weak variation of D with At at low density contrasts [also in Fig. 5(a)]. For instance, for $d=20$ mm, D is almost independent of At over a very broad range of values ($10^{-4}<\mathrm{At}<10^{-2}$). This contrasts with the very diverse qualitative properties of the flow regimes in that same range. The value of D in the low At regime increases also weakly with the tube diameter d (Fig. 5).

At higher density contrasts, D increases faster with At: the threshold At value for this increase gets lower for larger tube diameters d; the value of D for the highest Atwood numbers ($\mathrm{At}\gtrsim0.1$) may be slightly overestimated due to an increased viscosity of the higher density solution at large salt concentrations.

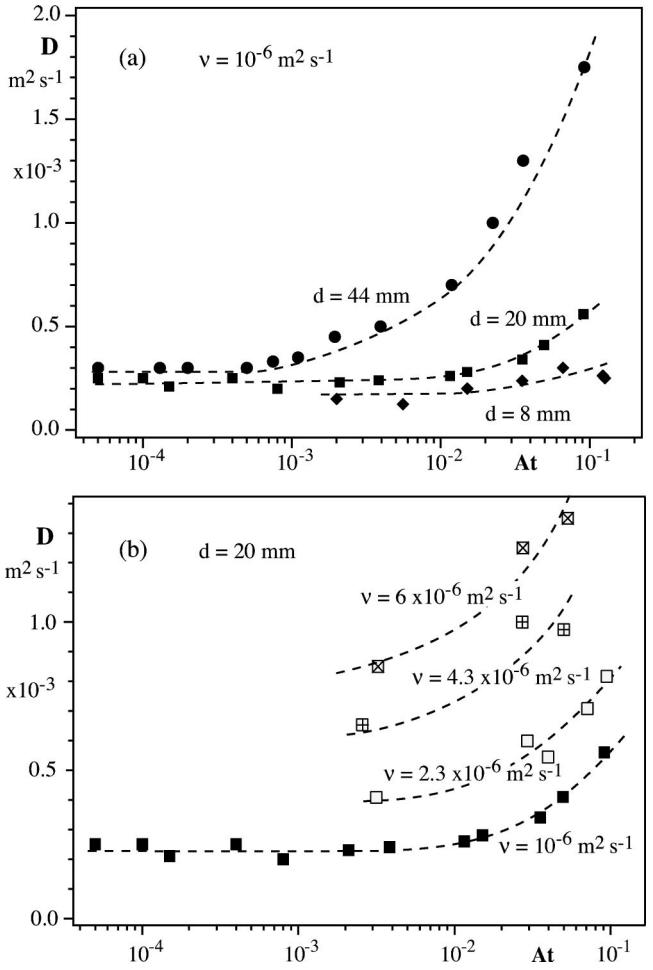

FIG. 5. (a) Variations of the macroscopic diffusion coefficient D as a function of the Atwood number At for three different tube diameters $d=44$ mm (●), $d=20$ mm (■), and $d=8$ mm (◆) ($\nu=10^{-6}$ m^2 s^{-1}). (b) The variation of D with At for fluid viscosities: $\nu=10^{-6}$ m^2 s^{-1} (■), 2.3×10^{-6} m^2 s^{-1} (□), 4.3×10^{-6} m^2 s^{-1} (⊞), and 6.0×10^{-6} m^2 s^{-1} (⊠) ($d=20$ mm). Dotted lines are only provided as guides for the eye.

Note that the large values of D reported above suggest a simple interpretation of the relatively slow fluid mixing, even at very large At values. An effective Rayleigh number $\mathrm{Ra}_{\mathrm{eff}}$ can indeed be defined by replacing in Eq. (1) the molecular diffusion coefficient D_m by the macroscopic coefficient D (this is a logical change since, in these flows, it is D and not D_m that characterize the interdiffusion of the fluids). $\mathrm{Ra}_{\mathrm{eff}}$ is lower than the threshold value Ra_c and one can consider that the system has reached a dynamical equilibrium in which no large scale instabilities can develop. Mixing results then only from the effect of the macroscopic diffusivity D.

2. Dependence on viscosity

Figure 5(b) displays variations of D with At in the 20 mm diameter tube for different viscosities between 10^{-6} and 6×10^{-6} m^2 s^{-1}. Surprisingly, D increases with the viscosity ν, implying that the mixing region between the two fluids spreads out faster for more viscous fluids. D increases by a factor of 4 for $\mathrm{At}\simeq10^{-2}$ when ν varies from 10^{-6} to 6×10^{-6} m^2 s^{-1}.

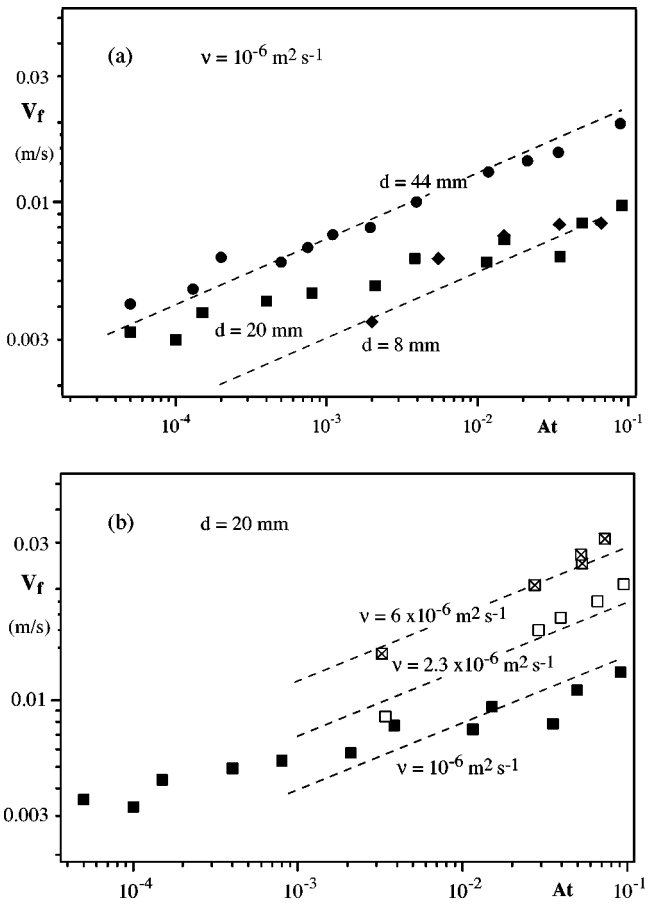

FIG. 6. The variation of V_f with At (a) for several tube diameters: $d=44$ mm (●), 20 mm (■) and 8 mm (◆). Viscosity $\nu=10^{-6}$ m^2 s^{-1}. (b) For several viscosities: $\nu=10^{-6}$ m^2 s^{-1} (■), 2.2×10^{-6} m^2 s^{-1} (□), 6.0×10^{-6} m^2 s^{-1} (⊠). Tube diameter $d=20$ mm. The slope of the dashed lines=0.25 [see Eq. (14)].

This influence of ν on D is much smaller at larger diameters: for $d=44$ mm, D still increases with viscosity but only by a factor 2.5 at low density contrasts ($\mathrm{At}\simeq10^{-4}$), while there is almost no variation at large ones ($\mathrm{At}\simeq10^{-1}$) (in both cases for an increase of viscosity by a factor of 4).

B. Experimental velocities of internal fluid motions

The previous results were derived from mean global concentration profiles measurements. At a more local scale, mixing and spreading of the two fluids is associated with random internal fluid motions in the mixing zone. The diffusivity D can be considered as the product $D=V_f\ell$ of their characteristic velocity V_f and a characteristic length ℓ as for every random walk process. These internal motions are directly visible in Figs. 2(a)–2(b). They are marked in the spatiotemporal diagrams of Figs. 3(a)–3(e) by oblique streaks of slope corresponding to V_f. Figure 6(a) displays in log–log coordinates the variation of V_f with At for $d=20$ mm and $d=44$ mm at a same viscosity $\nu=10^{-6}$ m^2 s^{-1}. V_f increases slowly with At for $\nu=10^{-6}$ m^2 s^{-1}. The variation of V_f with d is also slow: for a given Atwood number, the values obtained for $d=8$ mm and 20 mm are similar and only two times lower than for $d=44$ mm.

Figure 6(b) displays the variation of V_f with At in the tube of diameter $d=20$ mm for different viscosities. An unexpected feature is the increase of V_f with viscosity (by a factor of 5 for At=0.1) when ν varies from 10^{-6} m^2 s^{-1} to 6×10^{-6} m^2 s^{-1}. This increase of V_f with ν is probably related to that of D reported above. As for D, this effect is weaker for $d=44$ mm: V_f is still 100% larger at low density contrasts ($\mathrm{At}\simeq10^{-4}$) for $\nu=4.3\times10^{-6}$ m^2 s^{-1} while it is almost the same for $\mathrm{At}\simeq10^{-1}$.

Measurements of the macroscopic diffusion coefficient D and of the characteristic velocity V_f have provided therefore two particularly intriguing aspects. One is the weak dependence of D on the density contrast in spite of the broad range of At values investigated and the other the increase of V_f and D with viscosity.

It will be shown below that a possible explanation of these results is the fact that buoyancy forces that drive the mixing process are determined by local density contrasts $\delta\rho$ and not by the global density difference $\Delta\rho$. On the one hand, increasing At enhances mixing and reduces the ratio $\delta\rho/\Delta\rho$: this partly offsets the direct effect of the increase of the density contrast. On the other hand, increasing viscosity at a constant $\Delta\rho$ decreases the Reynolds number and leads to a coarser mixing: therefore $\delta\rho$ (and the buoyancy forces) increases.

V. DISCUSSION OF EXPERIMENTAL RESULTS

A. Characteristic velocities

1. Counter-current regime

In all flow regimes buoyancy forces are the driving mechanism. The stable counter-current regime observed at low At values may be modeled as a Poiseuille-like flow of the two unmixed fluids in opposite directions at a characteristic velocity V_c. Buoyancy forces per unit volume are of order $\Delta\rho g$ and are balanced by viscous forces of order $\rho\nu V_c/d^2$. V_c must then satisfy

$$V_c\simeq\frac{1}{48}\frac{\Delta\rho}{\rho}\frac{gd^2}{\nu}. \tag{3}$$

The factor 1/48 is obtained by approximating the flow in a circular pipe with the interface along a diameter. The shearing flow associated to this counter-current will become unstable at a certain value of the Reynolds number:

$$\mathrm{Re}_c=\frac{V_c d}{2\nu}\simeq\frac{g\,\mathrm{At}\,d^3}{48\nu^2}. \tag{4}$$

Experimental results displayed in Figs. 4(a)–4(b) indicate indeed that the value of At at the transition with the diffusive regime varies as d^{-3} and ν^2 as expected from Eq. (4). The corresponding critical value of Re_c is of the order of 130.

2. Diffusive regimes

In the convective–diffusive and turbulent–diffusive regimes, inertial rather than viscous forces balance buoyancy, leading to a new velocity scale:

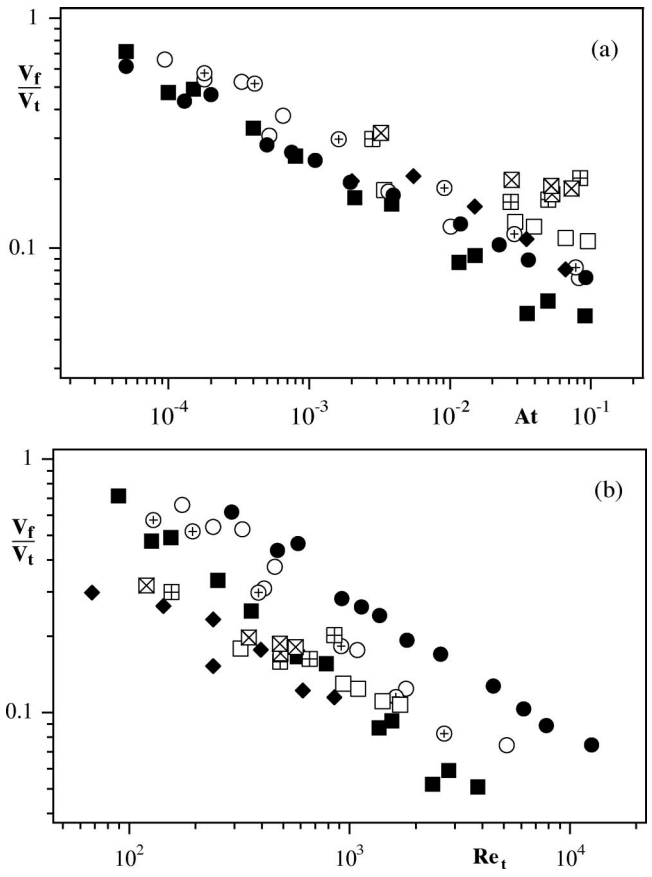

FIG. 7. Variation of the ratio V_f/V_t for several tube diameters $d=44$ mm: ●, ○, ⊕; $d=20$ mm: ■, □, ⊞, ⊠; $d=8$ mm: ◆ and several viscosities $\nu=10^{-6}$ m^2 s^{-1}: ●, ■, ◆; 2.3×10^{-6} m^2 s^{-1}: ○, □; 4.3×10^{-6} m^2 s^{-1}: ⊕, ⊞; 6.0×10^{-6} m^2 s^{-1}: ⊠—(a) variation of V_f/V_t as a function of the Atwood number At. (b) Variation of V_f/V_t as a function of the Reynolds number $\mathrm{Re}_t=V_t d/\nu$. The clear failure of the present plots (a) and (b) to provide a satisfactory collapse of the data using nondimensional parameters is discussed further in Secs. V A 2 and V B. This leads to a model discussed in Sec. V C which suggests an alternative plot (Fig. 9).

$$V_t=\sqrt{\frac{\Delta\rho}{2\rho}gd}=\sqrt{g\,\mathrm{At}\,d}. \tag{5}$$

This velocity corresponds to the fluid in an eddy being accelerated through a distance of $d/4$ starting from rest (the 1/4 factor is put for convenience to have a simpler expression of V_t). Figure 7(a) displays the observed V_f divided by this velocity scale V_t as a function of At. One first observes that the measured velocities are at most of the order of V_t, and more than one order of magnitude smaller at the highest values of At. Now, the vertical extension of the eddies, at least in the convective–diffusive regime, is greater than $d/4$ and often as high as several tube diameters [as observed in Figs. 2(b) and 2(e)]. Allowing the heavier fluid to accelerate through these large distances would lead to velocities higher than V_t rather than lower as observed in Fig. 7. Hence, one must conclude that local density differences $\delta\rho$ accelerating the flow are less than $\Delta\rho$.

Figures 6(b) and 7(a) also show a systematic increase of the velocity fluctuations V_f with increasing viscosity. As noted above, this is counter-intuitive. In the diffusive regime where $\mathrm{Re}_c>130$, frictional viscous forces should be negligible compared with inertial ones and so one should expect the velocity fluctuations to be independent of viscosity. If frictional forces were not entirely negligible, one would expect the velocity fluctuations to decrease with increasing viscosity. An explanation of this counter-intuitive trend must therefore be sought in terms of the viscosity decreasing the local Reynolds number (however larger than 1) which increases the local density differences. This discussion would not apply to fluids of very high viscosities: the Reynolds number is then low enough so that viscous forces slow down directly the fluid motion and reduce D and V_f. It is indeed observed that D no longer increases with viscosity for $\nu>10^{-5}$ m^2 s^{-1} and $d=20$ mm.

B. Nondimensionalization

Figure 7(a) plots the velocity fluctuations as a function of the Atwood number At which is a parameter that is easily adjusted in the experiments. While At has no dimension, it is not an appropriate nondimensional group. When the density contrast is small, one should use the Boussinesq approximation in which the inertial terms involve the average density and the buoyancy terms the varying density. Hence, the density difference $\Delta\rho$ only occurs when multiplied by the gravity acceleration g. Using the two other external parameters, the tube diameter d and the fluid viscosity ν, we can form only one nondimensional group. A second Reynolds number, now based on the velocity scale V_t and expected to be the relevant one in the diffusive regime, is therefore

$$\mathrm{Re}_t=\frac{V_t d}{\nu}=\sqrt{\frac{\mathrm{At}\,g d^3}{\nu^2}}=(48\,\mathrm{Re}_c)^{1/2}. \tag{6}$$

Figure 7(b) plots the observed velocity fluctuations V_f scaled by the inertial velocity V_t as a function of Re_t. We see that the data for different tube diameters and different fluid viscosities do not collapse onto a single curve: there are clear systematic variations from the average data as the diameter and viscosity change. This failure to collapse the data suggests that there must be another hidden parameter in the experiments. The molecular diffusivity D_m of the salt is more than three orders of magnitude smaller than the kinematic viscosity: it should therefore be irrelevant to mixing processes at the scale of the present experiments. Moreover, D_m has the same dimensions as the viscosity and would not help eliminate the systematic variations with the diameter in Fig. 7(b).

Despite this lack of success of dimensional analysis to collapse together the different velocity fluctuation curves, we consider now a nondimensional plot of the measured diffusivity D. In Fig. 8, D divided by the kinematic viscosity ν is plotted as a function of the second Reynolds number Re_t. In contrast with the previous case, the data points collapse onto a same global variation and two regimes are observed. For most experiments, corresponding to $\mathrm{Re}_t\lesssim1000$, the ratio D/ν is roughly constant and equal to 200: a large part of these data points corresponds to the convective–diffusive regime. The first order approximation $D/\nu=\cos t$ amounts to neglect the slow increase of D with the diameter d noted in Sec. IV A 1). At high Reynolds numbers ($\mathrm{Re}_t\gtrsim1000$), always cor-

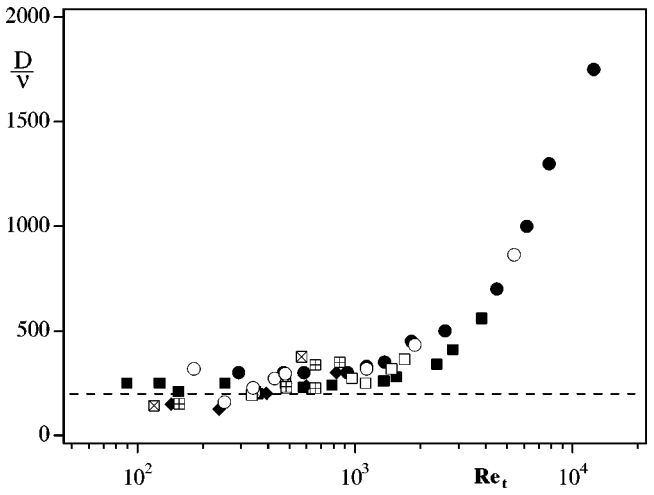

FIG. 8. Variation of the ratio D/ν with the Reynolds number $\mathrm{Re}_t = V_t d/\nu$ for tubes of diameters $d = 8$,20, and 44 mm and fluids of viscosities $\nu = 10^{-6}$, 2.3×10^{-6}, 4.3×10^{-6}, and 6.0×10^{-6} $\mathrm{m^2 s^{-1}}$. Horizontal dashed line corresponds to $D/\nu = 200$. Meanings of symbols are identical to those in Fig. 7.

responding to the turbulent–diffusive regime, D/ν increases with Re_t. In the following parts, we seek to account for these results.

C. Modeling the convective–diffusive regime

This section is devoted to a tentative model of mixing in the convective–diffusive regime ($\mathrm{Re}_t \lesssim 1000$) for which the ratio D/ν is constant and of the order of 200. As stated above, the local density fluctuations $\delta\rho$ determining the buoyancy forces driving convection are only a fraction of the global density difference $\Delta\rho$. This $\delta\rho$ can be taken equal to the variation in mean density over a distance ℓ which may be several tube diameters: ℓ represents the characteristic vertical size of an eddy or the typical extension of a convection event. Then

$$\delta\rho = \ell \frac{d\overline{\rho}}{dz}, \tag{7}$$

in which $\overline{\rho}$ is the average density at height z. If the global mixing region extends at a time t over a distance L, one may alternatively write

$$\delta\rho = \Delta\rho \frac{\ell}{L}. \tag{8}$$

Assuming that the local density fluctuation $\delta\rho$ accelerates from rest over the vertical distance ℓ, it will induce a velocity fluctuation V_ℓ of the order of

$$V_\ell = \sqrt{\frac{\delta\rho}{2\rho} g\ell} = \sqrt{\frac{\mathrm{At}\, g \ell^2}{L}}. \tag{9}$$

The distance ℓ is expected to increase with viscosity as the flow becomes more laminar and the vertical correlation length of the velocity fluctuations becomes longer. For similar reasons, the distance ℓ should also increase at low values of At. Assuming that eddies and/or convective motions develop through instabilities driven by inertial forces proportional to ρV_ℓ^2 balanced by viscous forces proportional to $\rho\nu/\tau$ (τ being the characteristic time scale for the growth of the instabilities) leads to

$$\frac{\rho\nu}{\tau} = C\rho V_\ell^2, \tag{10}$$

in which C is a numerical factor. The characteristic time τ may be expected to correspond to fluid displacements of velocity V_ℓ over a distance ℓ so that

$$\ell = V_\ell \tau. \tag{11}$$

Combining Eqs. (10) and (11) leads to the relation

$$C = \frac{V_\ell \ell}{\nu}, \tag{12}$$

between velocity fluctuations and the distance over which they remain correlated. On the other hand, the product of V_ℓ and ℓ should represent the diffusivity D associated with these fluctuations so that

$$D = V_\ell \ell = C\nu. \tag{13}$$

The experimental results displayed in Fig. 8 confirm this scaling law in the convective-diffusive regime with $C \simeq 200$. Eliminating l between Eqs. (9) and (12) leads to the scaling prediction

$$V_\ell = C^{1/2} \left(\frac{\mathrm{At}\, g \nu^2}{L} \right)^{1/4}. \tag{14}$$

The velocity scale V_ℓ may be expected to follow the same scaling law as the characteristic velocity V_f determined experimentally from spatiotemporal diagrams. Indeed, Eq. (14) predicts a slow increase of V_ℓ with viscosity and a slow variation with At as actually observed experimentally for V_f. The dashed lines in Figs. 6(a) and 6(b) represent the $\mathrm{At}^{1/4}$ variation in Eq. (14) and follow reasonably well the trends of the various data sets. The variation for $d = 20$ mm and $\nu = 10^{-6}$ $\mathrm{m^2\, s^{-1}}$ appears to be slower (the larger error on the determination of V_f at large At values may account in part for this discrepancy). The scaling law (14) is tested more quantitatively in Fig. 9 in which the ratio V_f/V_ℓ is plotted as a function of the Reynolds number Re_t for different tube diameters and fluid viscosities. The theoretical velocity V_ℓ is computed from Eq. (14) with $L = 1$ m which is an order of magnitude of the front width in the zones of the spatiotemporal diagram where V_f is generally determined. Values of the ratio obtained for $d = 8$ mm and 20 mm are nearly constant and close to 1 as expected ($V_f/V_\ell = 0.9 \pm 0.2$); those corresponding to $d = 44$ mm are also constant with Re_t but 50% higher.

D. Characteristic diffusion length

Combining Eqs. (9) and (12) also provides a scaling law for the characteristic length $\ell = D/V_\ell$,

$$\ell = C^{1/2} \nu^{1/2} \left(\frac{L}{\mathrm{At}\, g} \right)^{1/4}. \tag{15}$$

This prediction can be tested assuming that the experimental characteristic diffusion length D/V_f follows the same scaling

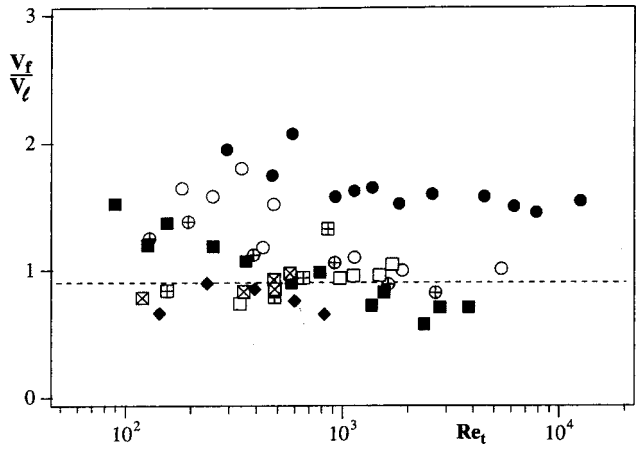

FIG. 9. Variation of the ratio V_f/V_l as a function of the Reynolds number Re_t for different tube diameters d and viscosities ν. The dashed line corresponds to an ordinate 0.9. Meanings of symbols are identical to those in Fig. 7.

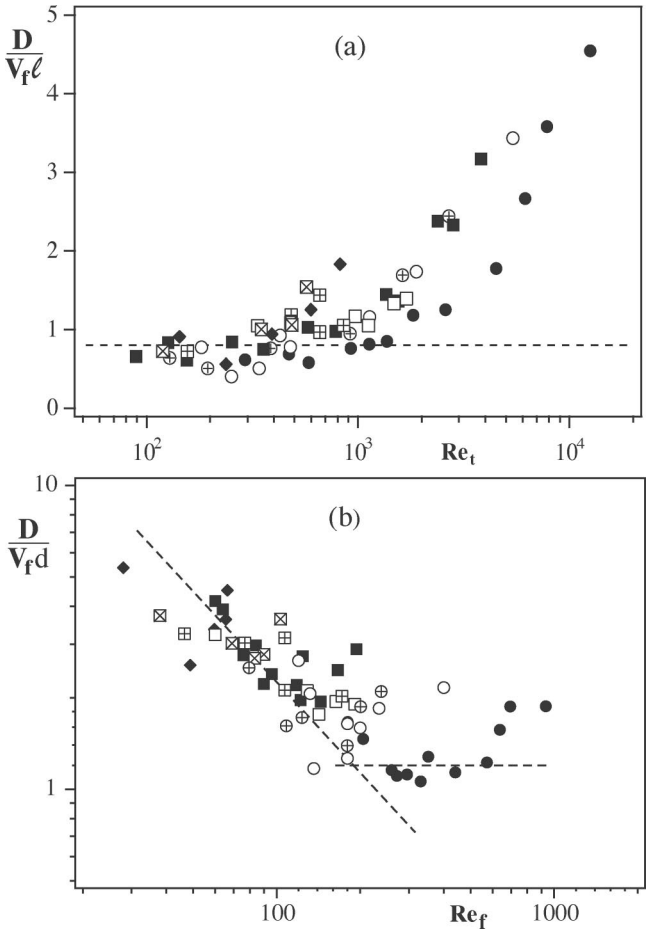

FIG. 10. (a) Variation of the ratio $D/V_f\ell$ with the Reynolds number Re_t for different tube diameters d and different fluid viscosities ν. The ordinate of the horizontal dashed line is 0.8. (b) Variation of the ratio D/V_fd as a function of the Reynolds number: $\mathrm{Re}_f=V_fd/\nu$ for the same set of experiments. Slope of the oblique dashed line $=-1$, ordinate of the horizontal dashed line $=1.2$. The meanings of symbols are identical to those in Fig. 7.

law as ℓ. Figure 10(a) displays variations of $D/V_f\ell$ as a function of the Reynolds number Re_t. The theoretical length ℓ is computed from Eq. (15) with the same value $L=1$ m as above. The ratio $D/V_f\ell$ remains globally constant and of the order of 0.8 ± 0.2 for all diameters and fluid viscosities over the same range of Reynolds numbers ($\mathrm{Re}_t\lesssim1000$) for which D/ν is constant (Fig. 8). This confirms the validity of the scaling law, at least in the convective–diffusive regime.

The diffusion length decreases with the Atwood number [see Eq. (15)] in this regime. It may be expected to have the tube diameter d as a lower limit when the turbulent–diffusive regime develops. In order to analyze this point, the normalized ratio D/V_fd is alternatively plotted in Fig. 10(b) as a function of a new Reynolds number $\mathrm{Re}_f=V_fd/\nu$. The ratio D/V_fd can be thought of as a ratio of an experimentally observed correlation length D/V_f to the tube diameter d while the new Reynolds number Re_f uses the observed velocities V_f rather than the overestimating theoretical V_t. Using Re_f instead of one of the previous definitions allows the collapse of the low Reynolds number data onto the same global trend [an oblique line of slope -1 in Fig. 10(b)]: the product $D/V_fd\times\mathrm{Re}_f$ is indeed equal to D/ν and therefore constant for $\mathrm{Re}_f\lesssim200$. For higher density contrasts, D/V_f no longer decreases and reaches values of the order of the tube diameter: $1.5d$ for $d=20$ mm and d for $d=44$ mm.

VI. CONCLUSION

The set of experiments reported in the present paper has confirmed that gravity-induced mixing in long vertical tubes is diffusive over a broad range of viscosities, density contrasts and tube diameters. Several characteristics of the process are, at first sight, unexpected, e.g., the increase of both the macroscopic diffusion coefficient D and the characteristic velocities V_f of the fluid motions with the fluid viscosity.

Using dimensional analysis, the variation of D with the global Reynolds number Re_t of the flow has demonstrated a transition between two diffusive mixing regimes. The variation of D with Re_t is faster for larger tube diameters and density contrasts—probably due to a weaker effect of the confinement by the tube walls.

An analysis of the spatiotemporal diagrams suggests a global picture of the phenomenon. A crucial point is that buoyancy forces inducing the flow are determined by the *local* density contrast $\delta\rho$ between moving fluid particles and the surrounding fluid rather than by the *global* contrast $\Delta\rho$ between unmixed fluids. The local contrast $\delta\rho$ depends not only on $\Delta\rho$ but also on the efficiency of mixing inside the flow which reduces density contrasts, and therefore buoyancy forces. This explains for instance the observed slow increase of the fluid velocities ($V_f\propto\mathrm{At}^{0.25}$ or slower) compared to the $\mathrm{At}^{1/2}$ dependence expected from Eq. (5). The effect of increasing $\Delta\rho$ is, in this case, largely compensated for by enhanced mixing.

For a constant $\Delta\rho$, both D and V_f increase with the viscosity ν. This does not reflect a *direct* effect of viscous forces: they are small compared to inertia and buoyancy forces in all cases. Viscosity has here an *indirect* effect by reducing the local Reynolds number Re_t (and slowing down mixing): there results an enhancement of the local density

contrasts and therefore of the buoyancy forces and, finally, an increase of V_f and D. A similar effect explains the slow variation of D with the tube diameter d: the decrease of the local Reynolds number Re_t results in poorer mixing and keeps the value of $\delta\rho$ high. Further fine scale measurements will however be needed to characterize more precisely the spatial and temporal characteristics of the fluctuations of the local concentration and fluid velocity: their dependence on ν, d and At are particularly important issues.

At low Atwood numbers, small tube diameters and high viscosities, the order of magnitude of the local density contrasts becomes of the order of that of the global one $\Delta\rho$. The scaling laws for the corresponding flow regimes remain to be identified. An important problem in this respect is the destabilization of the counterflow regime observed for very low density contrasts and the transition towards a diffusive regime.

The transition towards a stable counterflow regime may also be induced by inclining the tube from vertical. This issue is of great practical interest in such domains as chemical or petroleum engineering. The deviation induces a segregation of the lighter fluid in the highest parts of the tube section and helps to keep the two fluids separated. The domain of existence of the stable counterflow may then be considerably extended.

ACKNOWLEDGMENTS

We thank G. Chauvin, M. Delisée, R. Pidoux, and C. Saurine who designed and realized the experimental setup. We are indebted to G. M. Homsy for many illuminating discussions and contributions during his stay in the FAST Laboratory as an invited Professor of the Pierre and Marie Curie University. We also thank V. Fanguet and V. Rancillac for their contribution to the experiments. We are grateful to Dr. G. Daccord and the SRPC-Schlumberger Center who initiated and contributed to fund this research and to Professor A. Acrivos for useful suggestions.

[1]Lord Rayleigh, "Investigation of the character of the equilibrium of an incompressible heavy fluid of variable density," *Scientific Papers* (Cambridge University Press, Cambridge, 1900), pp. 200–207.
[2]G. K. Batchelor and J. M. Nitsche, "Instability of stationary unbounded stratified fluid," J. Fluid Mech. **227**, 357 (1991); "Instability of stratified fluid in a vertical cylinder," *ibid.* **227**, 419 (1991).
[3]S. Chandrasekhar, *Hydrodynamic and Hydromagnetic Stability* (Oxford University Press, Oxford, 1961), and references therein.
[4]D. H. Sharp, "An overview of Rayleigh–Taylor instability," Physica D **12**, 3 (1984).
[5]P. E. Linden, J-M. Redondo, and D. L. Young, "Molecular mixing in the Rayleigh–Taylor instability," J. Fluid Mech. **265**, 27 (1994).
[6]A. W. Cook and P. E. Dimotakis, "Transition stages of Rayleigh–Taylor instability between miscible fluids," J. Fluid Mech. **443**, 69 (2001).
[7]Y. N. Young, H. Tufo, A. Dubey, and R. Rosner, "On the miscible Rayleigh–Taylor instability: Two and three dimensions," J. Fluid Mech. **447**, 377 (2002).
[8]J. Fernandez, P. Kurowski, P. Petitjeans, and E. Meiburg, "Density driven, unstable flows of miscible fluids in a Hele-Shaw cell," J. Fluid Mech. **451**, 239 (2002).
[9]H.-J. Kull, "Theory of the Rayleigh–Taylor instability" Phys. Rep. **206**, 197 (1991).
[10]M. H. I. Baird, K. Aravamudan, N. V. Rama Rao, J. Chadam, and A. P. Peirce, "Unsteady axial mixing by natural convection in vertical column," AIChE J. **38**, 1825 (1992).
[11]E. E. Zukoski "A review of flows driven by natural convection in adiabatic shafts," NIST Report NIST-GCR-95-679, 1995, and references therein; J. B. Cannon and E. E. Zukoski, "Turbulent mixing in vertical shafts under conditions applicable to fires in high rise buildings," Technical Fire Report No. 1 to the National Science Foundation, California Institute of Technology, Pasadena, California, 1975.
[12]R. A. Wooding, "Growth of fingers at an unstable diffusing interface in a porous medium or Hele-Shaw cell," J. Fluid Mech. **39**, 477 (1969).
[13]S. B. Dalziel, P. F. Linden, and D. L. Young, "Self-similarity and internal structure of turbulence induced by Rayleigh–Taylor instability," J. Fluid Mech. **399**, 1 (1999), and references therein.
[14]R. A. Wooding, "Instability of a viscous liquid of variable density in a vertical Hele-Shaw cell," J. Fluid Mech. **7**, 501 (1959).
[15]N. A. Inogamov, A. M. Oparin, A. Y. Demy'anov, L. M. Dembitskioe, and V. A. Khokhlov, "On stochastic mixing caused by the Rayleigh Taylor instability," JETP **92**, 715 (2001).
[16]M. Debacq, V. Fanguet, J. P. Hulin, D. Salin, and B. Perrin, "Self-similar concentration profiles in buoyant mixing of miscible fluids in a vertical tube," Phys. Fluids **13**, 3097 (2001).
[17]G. I. Taylor, "The instability of liquid surfaces when accelerated in a direction perpendicular to their planes," Proc. R. Soc. London, Ser. A **201**, 192 (1950).
[18]G. I. Taylor, "Diffusion and mass transport in tubes," Proc. R. Soc. London, Ser. B **67**, 857 (1954).
[19]R. Bai, K. Chen, and D. D. Joseph, "Lubricated pipelining: Stability of core-annular flow. Part 5. Experiments and comparison with theory," J. Fluid Mech. **240**, 97 (1992) and references therein.
[20]J. Scoffoni, E. Lajeunesse, and G. M. Homsy, "Interface instabilities during displacements of two miscible fluids in a vertical pipe," Phys. Fluids **13**, 553 (2001).